Centrifuge Modeling of the Backward Erosion Piping Process

William Ovalle-Villamil,[1] and Inthuorn Sasanakul[2]

[1]University of South Carolina, Department of Civil and Environmental Engineering, 300 Main Street, Office C109, Columbia, SC 29208, United States; e-mail: wfo@email.sc.edu Corresponding author.
[2]University of South Carolina, Department of Civil and Environmental Engineering, 300 Main Street, Office C227, Columbia, SC 29208, United States; e-mail: sasanaku@cec.sc.edu

ABSTRACT

This study presents the application of the centrifuge modeling technique to model the backward erosion piping occurring in a sand layer under an impervious clay blanket subjected to field-stress conditions. Results from two centrifuge models with different circular exit-hole size are presented in this paper. The process is initiated through the exit-hole by gradually increasing the hydraulic gradient across the models. The evolution of global and localized hydraulic gradients along the seepage path is evaluated using pore pressure measurements, in-flight video recordings and post-failure observations. It is found that the critical global hydraulic gradient slightly increases as the size of the exit-hole increases. In addition, the local gradients developed differently depending on the exit-holes size, but the time elapsed during the erosion was similar. The critical local hydraulic gradients are much higher than the global values evidencing the importance of developing localized analyses to study backward erosion piping.

INTRODUCTION

The geotechnical centrifuge modeling technique is an innovative technique to develop parametric and nonparametric studies of geotechnical structures as an alternative to conventional small-scaled models and more complex full-scaled models. This technique allows simulating field conditions using small-scaled models by increasing the gravitational acceleration field. Despite the advantages of centrifuge modeling for research in geotechnical engineering, the use of this technique is limited for modeling backward erosion piping or other erosion mechanisms. Consequently, there is a lack of experimental data that facilitates the interpretation of existing results from centrifuge models and their extrapolation to field conditions.

The lack of experience in centrifuge modeling of backward erosion piping is due to the challenge of developing reliable models that combine simultaneously different complex mechanisms, such as flow in different directions and erosion (Wibowo et al. 2016). Nonetheless, the main difficulty arises from the limitations that have been identified using theoretical assessments. For instance, the work of Goodings (1982, 1984) analyzed the effects of increasing the gravitational acceleration field in small-scale models of erosion. It was indicated that

reductions in the grain-size of the soil used in the model, relative to that in the field, may be required to ensure similarity for centrifuge modeling. Such changes in grain-size may be inconvenient due to the consequent change in the soil properties that govern the mechanics of flow and erosion in the model. Other theoretical works show more promising strategies to develop centrifuge models of erosion (e.g., Bezuijen and Steedman 2010; Dong et al. 2011), but some aspects in the models are still considered problematic, such as the effect of centrifuge gravitational acceleration in certain time-related variables, such as the rate of erosion. Although these theoretical works focused in both surface and internal erosion mechanisms, to the best of the authors' knowledge, experimental validation applicable to specific types of erosion, such as backward erosion piping, has not been developed with enough detail in the literature.

This paper presents preliminary experimental results obtained from centrifuge models of backward erosion piping and provides new insights into the centrifuge modeling of this phenomenon under an increased gravitational acceleration field. The models simulate the erosion process that initiates at an exit point near the downstream toe of a dam or levee and then progresses backwards through a sand foundation towards the impoundment. The main objectives of the study are to observe the development of the phenomenon within centrifuge models and to assess the critical hydraulic conditions triggering the phenomenon.

BACKGROUND

A summary of the research studies involving centrifuge modeling of backward erosion piping is presented in this section. Van Beek et al. (2010) developed an investigation of backward erosion piping in centrifuge models to observe the influence of increments in the gravitational acceleration field or g-level. The first model composed of a sand foundation underlain by a plastic plate cover was tested at 30g by increasing the hydraulic gradient across the specimen until sand transport was observed. The total seepage length and the thickness of the sand foundation were 35 cm and 10 cm, respectively, and an open exit was used to initiate the erosion (Bonelli 2013). The second model resembling a levee system with similar dimensions and exit condition was also tested at 80g. The critical global hydraulic gradients obtained in the first and second models were 0.33 and 0.23, respectively. This study showed that the critical values decreases as the g-level increases due to the development of nonlaminar flow across the piping path.

A similar study was conducted by Leavell et al. (2014) including three centrifuge models at different levels of gravitational acceleration. The first two models simulated a levee foundation with 12.7 cm in thickness and 96.5 cm in length. A clay blanket with 2.5 cm in thickness was placed on top of the models and an exit-hole with 0.9 cm in diameter was used to initiate the erosion at a distance of 45.7 cm from the upstream reservoir. The third model had the same dimensions, but the thickness of the foundation was reduced by 2.5 cm and an additional clayey sand layer was added between the foundation and the clay blanket. Although values of critical hydraulic gradients are not reported in this study, post-failure visual observations of the

three models showed that piping only occurs on the surface of the foundation. This study also highlighted that centrifuge models of backward erosion piping should be designed to be simplistic and to minimize the g-level as the scale effects become more significant as the g-level increases.

Koito et al. (2016) developed a descriptive study of backward erosion piping in centrifuge models by modeling two levee systems with 20 cm in length and 5 cm and 2.5 cm in thickness of foundation soil. Both centrifuge models were tested at 50g and an open exit was used to initiate the erosion. The critical global hydraulic gradients obtained increased as the thickness of the foundation decreased, with average values of 0.214 and 0.333 for thickness values of 5 cm and 2.5 cm, respectively. This study highlighted that multiple piping paths with meandering behaviors may develop in the models, and the critical path does not necessarily follow the shortest seepage path (Horikoshi et al. 2019).

EXPERIMENTAL METHODOLOGY

The tests were performed in a 1.3 m–radius geotechnical centrifuge using the setup shown in Fig. 1. The centrifuge model container is made of aluminum and consists of three chambers. The models are placed in the middle chamber and the two side chambers are used as upstream and downstream reservoirs. The middle chamber has dimensions of 31.5 cm in length, 31.5 cm in width, and 30 cm in height. A porous plate and a no. 200 mesh are placed between the middle chamber and the side reservoirs to allow uniform distribution of flow during tests.

The soil tested in this study is Nevada sand, with a rounded particle-shape, a uniform gradation (Cu=1.54; Cg=0.95) and an effective diameter of 0.13 mm. As shown in Fig. 1, the models consist of a sand foundation, prepared by compacting 4 layers of dry sand to achieve 9 cm in height, and an impervious blanket made of clay with 2.5 cm in thickness. The clay material is a moist pottery clay, and it is used to provide overburden stress to the sand foundation. A cylindrical exit-hole is perforated on the clay blanket at a distance of 15 cm from the upstream reservoir, and it is used to initiate the backward erosion piping. The saturation of the sand model is done by applying low increments of the water level in the downstream reservoir until a final elevation of 10 cm above the bottom of the container is obtained across the models.

A total of five piezoresistive miniature pressure transducers with measuring range from 0 to 350 kPa are installed at the interface between the sand and clay layers to monitor the pressure losses in different segments of the model, and a video camera is placed above the exit-hole to observe the model behavior during the test. The test is performed by gradually increasing the water level in the upstream reservoir while maintaining a constant water level of 10 cm in the downstream reservoir. The process is to induce horizontal flow across the specimen in small increments of gradient. The global hydraulic gradient, i_{global}, resulting from the head loss between the upstream and downstream reservoirs, is used as test control. Several increments of i_{global} are applied until the water level in the upstream reservoir can no longer be maintained or

increased. This is the indication of the backward erosion piping failure. Two centrifuge models, namely Models A and B, with exit-hole size, D, of 2.6 cm and 1.8 cm, respectively, were tested in this study.

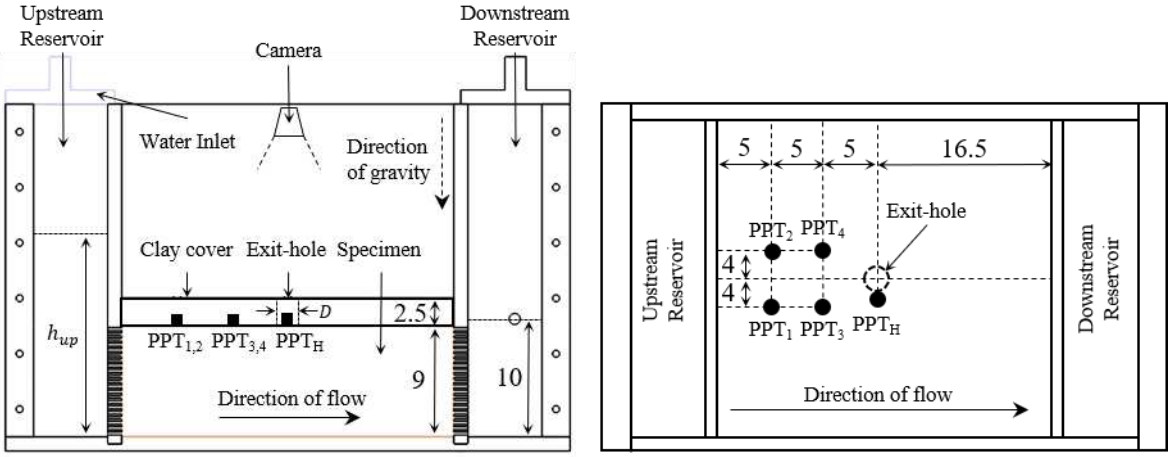

Figure 1. Lateral and plan views of experimental setup (units in cm).

RESULTS AND DISCUSSION

This section presents the visual observations and analysis of the results obtained from two centrifuge models tested at a g-level of 10g. The sand surface is subjected to approximately 5 kPa of field overburden stress. Visual observation via centrifuge onboard camera is presented first and is followed by the results from pore pressure sensors. The backward erosion piping behavior observed in centrifuge environments is discussed.

Visual observations of backward erosion piping in a centrifuge model

The video recordings obtained during the centrifuge tests were evaluated to assess the different stages of the erosion process by identifying changes at the exit-hole location. Fig. 2 presents the observations in Model A. In Fig. 2a, the initial condition at the exit-hole before any increment of i_{global} is shown. The water level inside the exit-hole is initially 1 cm above the surface of the sand layer. As i_{global} increases, the water level inside the exit-hole increases indicating that the upward flow occurs across the hole. This behavior implies that the 2-dimensional flow is anticipated in the sand foundation, with the upward flow across the exit-hole and the horizontal flow across the entire seepage length. However, after each increment of i_{global}, the water level inside the exit-hole reaches a new constant elevation and the flow across the sand foundation is mainly horizontal after equilibrium is achieved, as shown in Fig. 2b. This behavior repeats for every increment of i_{global} until the water level inside the exit-hole exceeds the surface of the clay blanket and the flow remains 2-dimensional until the end of the test, as shown in Fig. 2c.

After a continuous upward flow condition across the exit-hole is established and at a certain level of i_{global}, sand particles dragged by the flow of water become visible indicating that

the erosion has begun. The initial erosion is visually identified by suspension of small amounts of grains above the exit-hole, as shown in Fig. 2d. The erosion progression is observed with the increased amount of suspended sand particles, as shown in Fig. 2e. Afterwards, the erosion rate increases and a more significant amount of eroded sand is observed, as shown in Fig. 2f. The general behavior shown in Figs. 2d, 2e and 2f indicates that a piping path started at the exit-hole and progressed towards the upstream reservoir. The piping path eventually reached a critical length near the upstream reservoir resulting in a preferential flow path between the upstream reservoir and the exit-hole. This leads to a widening process across the piping path as observed with the significant amount of eroded sand. At this point, the model is considered failed.

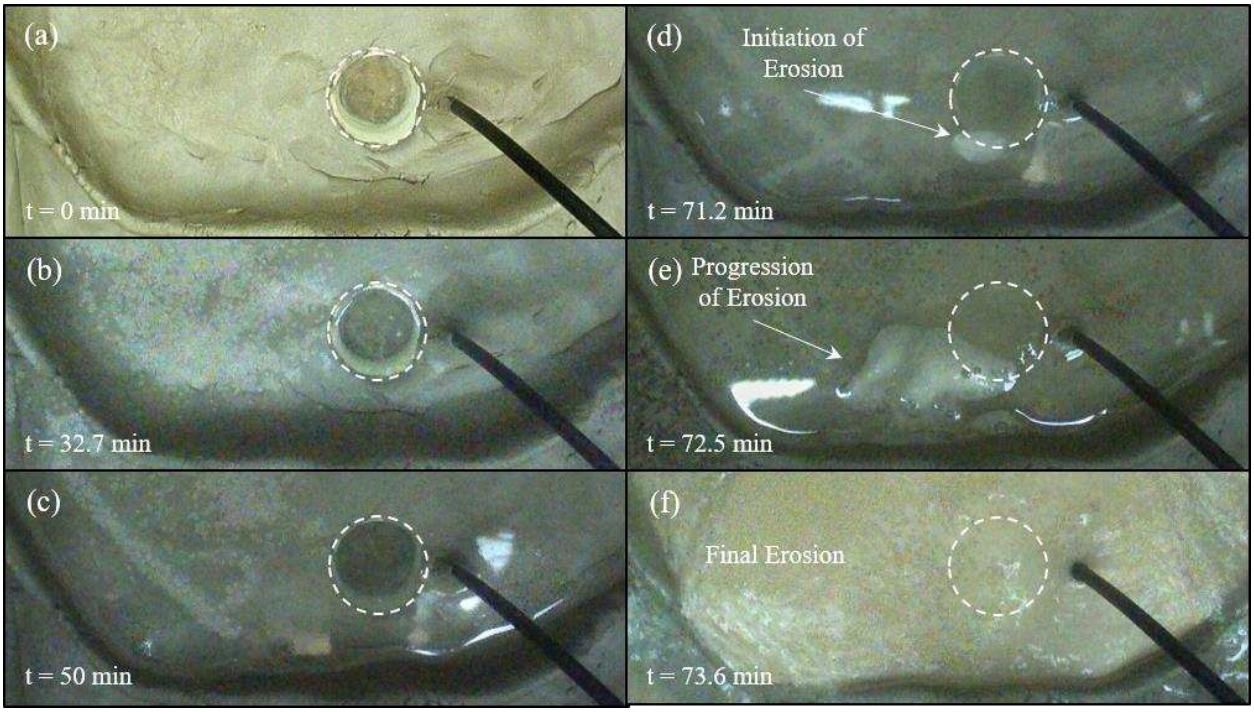

Figure 2. Evolution of backward erosion piping in centrifuge model A.

After the test finished and the centrifuge stopped, the clay blanket was carefully removed for visual inspection of the erosion pattern. Fig. 3a shows a top view of Model A, and Fig. 3b shows a close-up view of the eroded zone. It is observed that only the section between the exit-hole and the upstream reservoir was eroded, while there were no signs of erosion downstream from the exit-hole. This observation verifies that the backward erosion piping occurred in the centrifuge model. In contrast to the observations by Koito et al. (2016), the erosion occurred towards the center of the sand model and the piping path appears to follow the shortest distance between the exit-hole and the upstream reservoir, with minimum meandering behavior. This may be justified considering that the open space exit used by Koito et al. (2016) allows the formation of several parallel piping paths with different exits for grain transport, while the circular exit-hole type used in this study forces the erosion to begin from a singular location and the grains to be ejected through the same location. Post-test evaluation show that the widened path has 7.5 cm

in width at the location of the exit-hole and ranged from 4.5 cm up to 5.5 cm across its length. The average depth of erosion is 0.5 cm across the piping path and appears to be uniform across the model. It is noted that Leavell et al. (2014) observed similar behavior regarding the depth of the erosion with an average value of 0.8 cm.

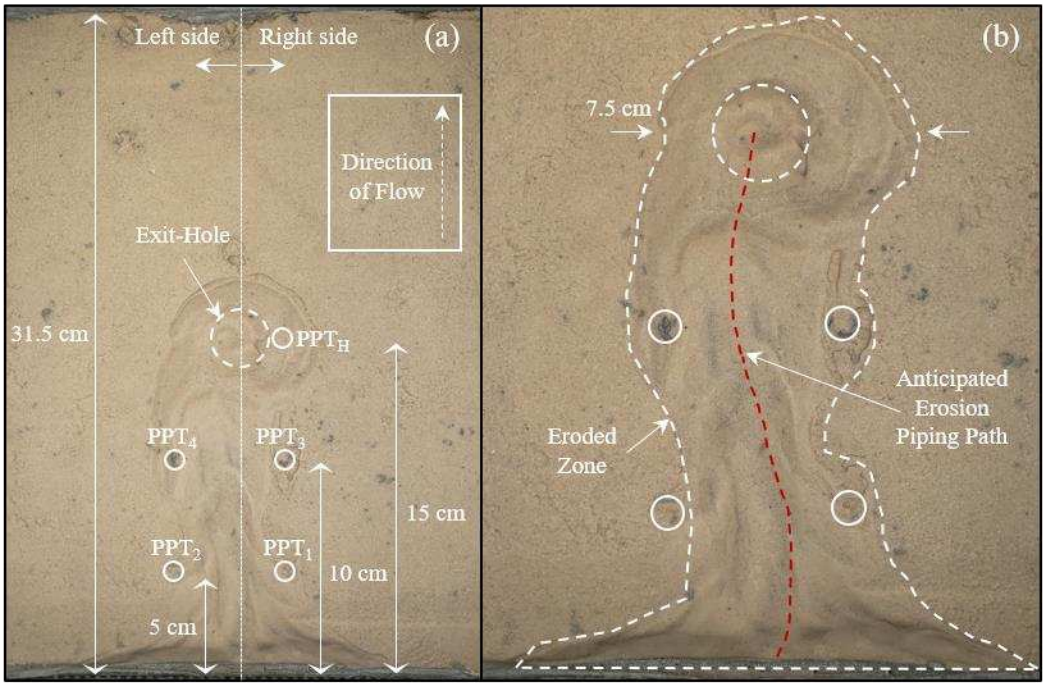

Figure 3. Post-failure state of Model A: (a) total surface and (b) erosion zone.

Pressure evolution during the backward erosion piping in a centrifuge model

Fig. 4 shows the evolution of the pore pressure, P, as a function of the time measured at several locations in Model A. The magnitude of i_{global} and the times associated with continuous upward flow across the exit-hole, as well as the initial and final erosions, are shown. As seen in Fig. 4a, the values of P at each location increases for every increment of i_{global}. The values of P are the greatest at the locations near the upstream reservoir and the lowest near the exit-hole. This behavior is expected because the pressure loss increases as the seepage length from the upstream reservoir increases. It is interesting to highlight that the values of P at PPT_1 and PPT_2, located at 10 cm away from the exit-hole, are similar throughout the test, while slightly different values of P were measured at PPT_3 and PPT_4, located at 5 cm away from the exit-hole. For the latter distance, the magnitude of P is greater towards the right side of the model than in the left side (see Fig. 3a). This behavior indicates that the flow may become less symmetrical with reference to the central axis of the model as it gets closer to the exit-hole. It should be noted that this behavior may be also due to the non-uniform distribution of porosity near the surface of the sand foundation.

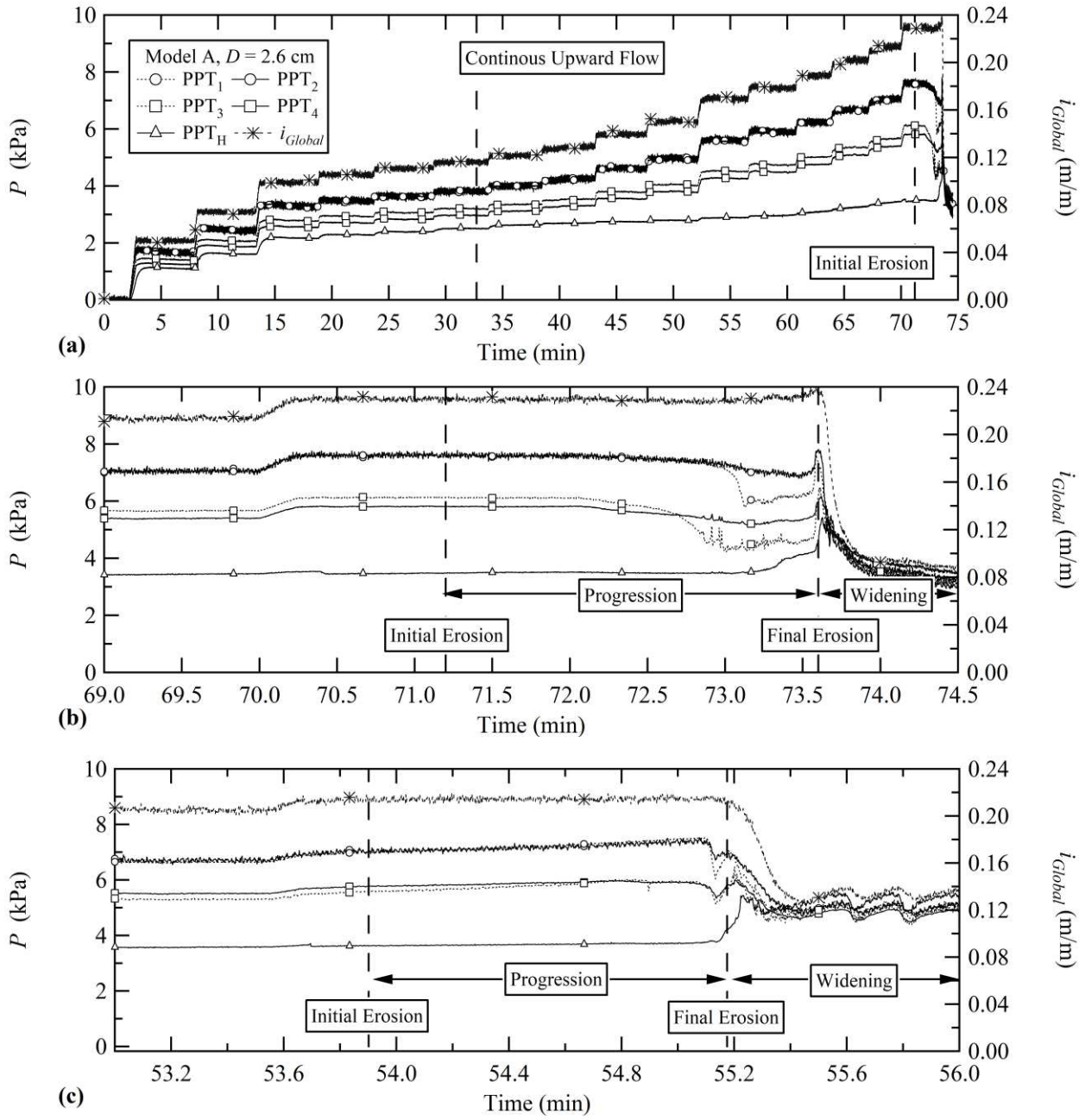

Figure 4. Evolution of pressure readings: (a) total duration of test and (b) last increment of i_{global} in Model A, and (c) las increment of i_{global} in Model B.

Fig. 4b shows a zoomed plot of Fig. 4a for the last increment of i_{global}. With exception to the value of P at PPT_H located at the exit-hole, the values of P in all locations decrease after the initial erosion is visible in the video recordings. This decreasing behavior is first observed at PPT_3 and PPT_4 at nearly 72.1 minutes of test. The value of P at PPT_3 decreases at a greater rate compared to PPT_4 and reaches a fairly constant lowest value at nearly 72.9 minutes. There is no change in the value of P at PPT_H during this interval of time, thus there is a localized decrease in

the pressure loss between the location of PPT3 and PPT4 and the exit-hole. Nonetheless, the pressure loss across the entire seepage length remains as there is no noticeable change in the other locations or in the reservoirs. This behavior indicates that a piping path has initiated at the exit-hole and extended approximately 5 cm towards the upstream reservoir.

Immediately after the time of 72.1 minutes, the value of P at PPT_1 and PPT_2 starts to decrease, while the value of P at PPT_H starts to increase. The value of P at PPT_1 shows a greater rate of decrease compared to PPT_2 at 73 minutes and continues until reaching the lowest value at 73.2 minutes (12 seconds later). This behavior indicates that the piping progressed to reach the location of PPT_1 and PPT_2, but the piping length had not reached the upstream reservoir as no change is observed for i_{global} and for P at PPT_H. Between the times of 73.2 minutes and 73.5 minutes, the rate of increase of PPT_H increases sharply while there is no abrupt change in the value of P at other locations. The behavior observed in this interval of time implies that the pressure loss across the entire specimen has decreased as less pressure is lost between the upstream reservoir and the exit-hole. It is of note that the greatest decrease of P during the development of backward erosion piping was experienced towards the location of PPT_1 and PPT_3. This behavior indicates that the piping path may have progressed closer to the location of these two pressure ports.

At 73.6 minutes, the piping path progressed backwards to reach the upstream reservoir (or a critical length) and led to the final erosion. At this moment, the flow concentrates in the piping path as observed from the sudden increase of P at every location, and then abruptly decreases. This indicates that the pressure loss is completely diminished across the specimen and the failure of the sand foundation occurred as observed from i_{global} that also decreased. The total time elapsed between initial and final erosion was approximately 2.4 minutes and 2.1 minutes for Models A and B, respectively.

The general behavior observed with Model A is also replicated in Model B with a few exceptions during the progression phase, as shown in Fig. 4c. First, the evolution of P is rather similar at PPT_1 and PPT_2, and at PPT_3 and PPT_4, indicating that the piping path may have progressed across the center of the specimen. Second, the decrease of P at PPT_3 and PPT_4 at 54.7 minutes of test, indicating that the piping has progressed towards the location of these sensors, presents a lower rate compared to Model A. Finally, the piping path appears to reach the location of PPT_1 and PPT_2 at 55.1 minutes as P at these locations decreases sharply. However, this decrease occurs simultaneously at PPT_3 and PPT_4, and the final erosion occurs only four seconds after. This behavior indicates that the critical length of piping may be equivalent to the distance between PPT_1 and PPT_2 and the exit-hole, and it is likely shorter than in Model A.

Evolution of local hydraulic gradients

To assess the behavior of the flow in both global and local perspectives, the hydraulic gradient was calculated for different segments using the pressure readings shown in Fig. 4. In addition to i_{global}, two sets of localized hydraulic gradients are assessed in this study. Firstly, the hydraulic

gradients across the segments closest to the exit-hole, i_{3-H} and i_{4-H}, obtained with the pressure readings at PPT_3 and PPT_4, respectively, and the pressure reading at PPT_H. Secondly, the hydraulic gradients across a longer segment, i_{1-H} and i_{2-H}, obtained from PPT_1 and PPT_2, respectively. Fig. 5 shows the evolution of i_{1-H}, i_{2-H}, i_{3-H} and i_{4-H}, as functions of i_{global}, obtained with Model A. The figure is discretized to account for variations on each side of the specimen.

For a range of i_{global} between 0 and 0.10, the local hydraulic gradients sharply increase in response to the increase in i_{global} and then decrease to reach equilibrium, as shown in Figs. 5a and 5b. As described previously, and as shown in Fig. 2, this behavior is likely related to the transition from a combined upward and horizontal flow condition to solely a horizontal flow condition that occurs for each increment of i_{global} while the stabilized water level inside the exit-hole remains below the surface of the clay blanket. Once the continuous 2-dimensional flow exists in the test when the i_{global} is greater than 0.12, the increasing of the local hydraulic gradients is less scattered regardless of the location in the model.

As shown in Fig. 5a, the local hydraulic gradients in the segments on the left side of the model are similar until the initial erosion occurs (i.e., $0.12 > i_{global} > 0.23$). In contrast, for the same range of i_{global} the gradient in the segment closest to the hole, i_{3-H}, is noticeably greater than that in the longer segment, i_{1-H}, as shown in Fig. 5b. This behavior could be due to soil loosening near the exit-hole and flow concentration towards the right side of the model. Consequently, there is a greater pressure loss in the segment between PPT_3 and PPT_H than in the segment between PPT_1 and PPT_H. The initial erosion takes place when the local hydraulic gradients reach a peak value. Afterwards, the local hydraulic gradients consistently decrease in every segment. This behavior indicates that even though a constant value of i_{global} governs the flow across the specimen, changes in local gradients take place as the piping progresses. These localized changes represent the progression of piping erosion. After the final erosion occurs, the local and global hydraulic gradients decrease significantly. Consequently, the sand foundation is incapable of retaining water in the upstream reservoir.

To assess the critical conditions leading to the backward erosion piping, the critical hydraulic gradient, i_{cr}, was estimated from the pressure readings and visual observations of Models A and B. The assessment includes two main events observed during the test: (1) initial erosion and (2) final erosion. The critical local hydraulic gradients are determined for the shortest segments of 5 cm nearest to the exit-hole, for the longest segments of 10 cm from the exit-hole and for the entire seepage length. Results are presented in Fig. 6. It is highlighted that the critical hydraulic gradient is usually defined for the entire seepage length in the literature, therefore it is referred to as the critical global hydraulic gradient. In this study, the critical local hydraulic gradients are also presented.

The initiation, progression, and final failure occurred for the same value of i_{global} in both Models A and B, as described in Fig. 5. The average values of critical global hydraulic gradient were approximately 0.22 and 0.24 for values of D of 1.8 cm and 2.6 cm, respectively. These results may not be comparable with those obtained by van Beek et al. (2010) and Koito et al.

(2016) due to several factors, including, but not limited to, the differences in centrifuge gravity, effects of model dimensions, and characteristics of the materials. Nevertheless, the critical values obtained in this study fall into the same range of values reported.

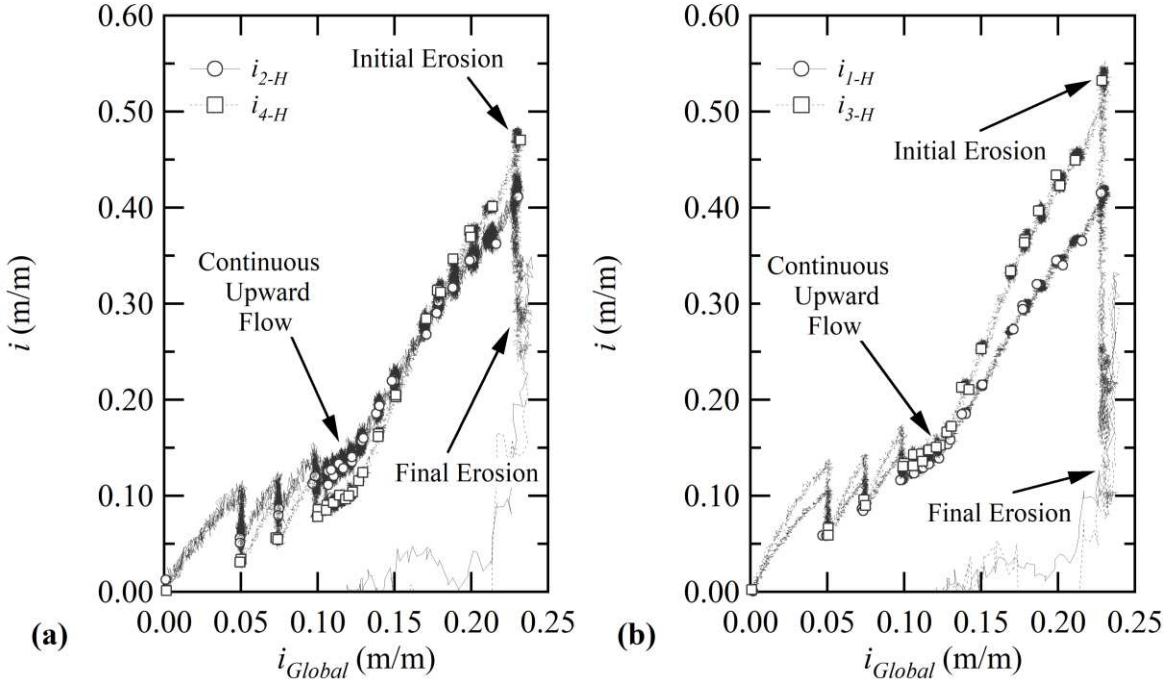

Figure 5. Evolution of local and global hydraulic gradients: (a) left and (b) right sides of Model A.

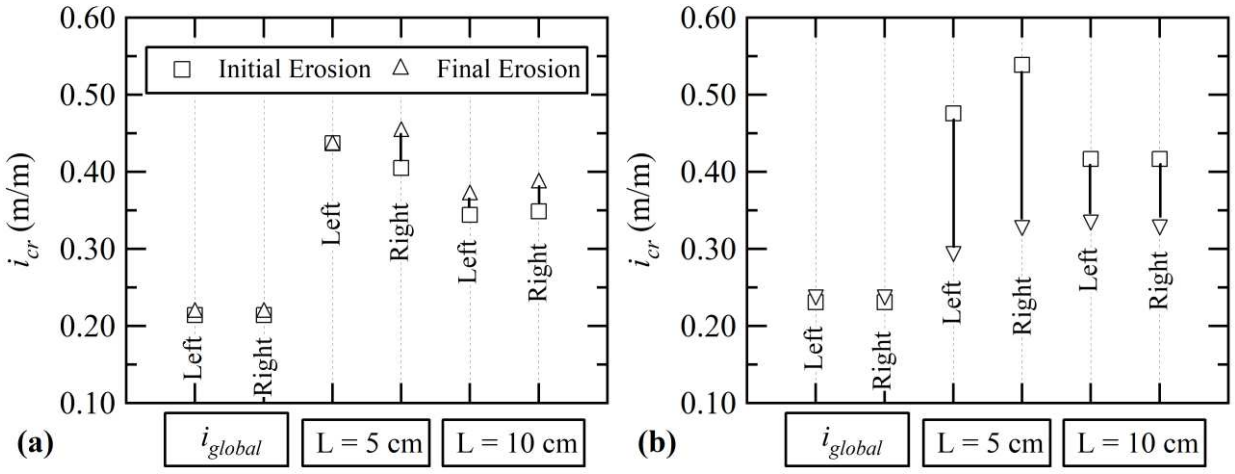

Figure 6. Critical global and local hydraulic gradients: (a) $D = 1.8\ cm$ and (b) $D = 2.6\ cm$.

For the initial erosion, the local critical hydraulic gradient across the distance of 10 cm from the exit-hole, was observed to be increased as D increased, with values of 0.35 and 0.42 for values of D of 1.8 cm and 2.6 cm, respectively and regardless of the location in the model.

Greater values of critical hydraulic gradients were obtained for the shortest distance of 5 cm from the exit-hole, with values of 0.40 and 0.44 for $D = 1.8\ cm$, and 0.48 and 0.54 for $D = 2.6\ cm$. As seen, the location of the segment has a significant impact on the local critical hydraulic gradient. For instance, the value obtained in the shortest segment is nearly two times the global value. Such difference demonstrates the importance of localized analyses to improve the understanding of the initiation and progression of backward piping erosion.

Different behavior was observed for the evolution from initial to final erosion when comparing results between Models A and B. For $D = 1.8\ cm$ (Model B), the hydraulic gradient increased from the initial erosion to the final erosion, while the opposite behavior was experienced for the test with $D = 2.6\ cm$ (Model A). The soil grains appear to be more easily removed as the exit-hole size increases. This behavior could be related to how the grains transported in each model. For Model B, the amount of transported grains during the initiation of erosion is less than that of Model A. Hence, the gradient across the model decreases after the initial erosion in Model A because there is less material left in the seepage path, hence low porosity and less resistance against flow. In contrast, the material may accumulate in the exit-hole causing a consistent increase in hydraulic gradient in Model B.

CONCLUSIONS

This study presents the results and observations of two centrifuge models of the backward erosion piping initiated by a circular exit-hole with different diameter. An initial seepage phase is identified with an intermittent transition between combined upward and horizontal flow and individual horizontal flow. When the water level in the upstream reservoir is high enough, a combined flow condition is established and continues until the erosion initiates, progresses, and causes the failure of the models. Post-failure observation shows that the piping path is developed at the surface of the sand foundation with an average depth of 0.5 cm. Although only the widened path could be observed after the test, the piping path occurs along the shortest distance between the exit-hole and the upstream reservoir with minimum meandering behavior.

Critical global and local hydraulic gradients across different segments of the surface of the foundation sand are measured in this study. It is found that the critical global hydraulic slightly increases as the diameter of the exit-hole increases. Although the time elapsed from the initial erosion to the failure is similar in the models, the evolution of local hydraulic gradients is dependent on the exit-hole size. For both models, the critical local hydraulic gradients are greater than the global values and the difference increases as the local seepage length decreases. Although direct comparison with the literature should be done with caution, some key observations and results shown in this study compare reasonably well with results from previous centrifuge models tests.

REFERENCES

Bezuijen, A., and Steedman, R. S. (2010). "Scaling of hydraulic processes". In *Proceedings of the 7th international conference on physical modeling in geotechnics*, Taylor and Francis Group, London, UK.

Bonelli, S. (2013). "Erosion in geomechanics applied to dams and levees". *ISTE*, London.

Dong, P., Newson, T. A., Davies, M. C. R., and Davies, P. A. (2001). "Scaling laws for centrifuge modelling of soil transport by turbulent fluid flows". *International Journal of Physical Modelling in Geotechnics*, 1(1), 41-45.

Goodings, D. J. (1982). "Relationships for centrifugal modelling of seepage and surface flow effects on embankment dams". *Géotechnique*, 32(2), 149-152.

Goodings, D. J. (1984). "Geotechnical Centrifuge Modeling of Soil Erosion." *Transportation Research Record*, 998, 1.

Horikoshi, K., Noda, S., Takizawa, A., and Takahashi, A. (2019). "EWG-6 Centrifuge Modeling for Visualization of Backward Erosion Piping Progression". In *Book of Abstracts,* pp. 17.

Koito, N., Horikoshi, K., and Takahashi, A. (2016). "Physical modelling of backward erosion piping in foundation beneath levee". *Scour and erosion*, 445-451.

Leavell, D. A., Wibowo, J. L., Yule, D. E., and Strange, R. C. (2014). "Geotechnical centrifuge experiments to evaluate piping in foundation soils (No. ERDC/GSL-TR-14-14)". *Engineer Research and Development Center Vicksburg MS Geotechnical and Structures Lab*.

Van Beek, V. M., Bezuijen, A., and Zwanenburg, C. (2010). "Piping: Centrifuge experiments on scaling effects and levee stability". *Physical Modelling in Geotechnics*, ISBN 978-0-415-59288, 8, 183-187.

Wibowo, J. L., Robbins, B. A., Wilhelms, S. C., and Leavell, D.A. (2016). "Centrifuge Modeling of Levee Breaches: Is it possible?" *Eurofuge*, Nantes, France.